

# Modeling and Simulation of a Periodic Grating Coupled Configuration for Surface Plasmon Excitation

Helmut F. Schiretz and Abbas Z. Kouzani

*School of Engineering  
Deakin University*

*Geelong, Victoria 3217, Australia*

hschi@iprimus.com.au & kouzani@deakin.edu.au

**Abstract** - The deficiencies in the design of surface plasmon resonance (SPR) systems that are reported in numerous published works consistently identify the optics assembly as the main problem in the miniaturization of SPR sensors for integration into biosensor systems. This paper presents a novel design of a grating coupled optical waveguide surface plasmon (SP) excitation mechanism, investigated with the intention of addressing the problems associated with using the traditional prism input-output light coupling approach. Computational multiphysics modeling and simulation of the design is carried out. The results are presented and discussed.

**Index Terms** – *Biophotonics, biosensors, plasmon, optical surface waves, gratings.*

## I. INTRODUCTION

Most surface plasmon spectroscopy (SPS) instruments are based upon an attenuated total reflection (ATR) prism-coupling mechanism called the Kretschmann configuration of [1], which is well suited for large application platforms in laboratories. However, this mechanism suffers from significant deficiencies in its application and suitability for small field deployable biological analysis instrumentation. The theory behind SPR is described in [2].

The deficiencies in a design posed for a portable SPR biosensor by CSIRO researchers of [3, 4], highlighted that the prism-coupling optic assemblies provide the greatest system integration problems for portable handheld field deployable SPR analytical instrumentation, particularly in the requirement for a cumbersome dielectric index-matching coupling mechanism.

Another inherent problem in designing field deployable SPR instrumentation is that commercial systems are not designed to use disposable sensing devices as they are invariably based on a glass substrate which complicates the integration of the sensor device and a fluid cell as explained in [3, 4].

The aim therefore is to address the problems associated with using the traditional prism input-output light coupling approach. Computational multiphysics modelling and simulation of the design is carried out.

The chosen option for investigation and modelling is an optical waveguide device designed based on a “bi-directional” grating coupler model, using a polycarbonate (PC) substrate, details of which are outlined in following sections.

The paper is organized as follows. Section II describes the development of the model. Section III presents multiphysics

modeling and associated results. Section IV provides a discussion of the results. Section V gives concluding remarks.

## II. MODEL DEVELOPMENT

### A. Principle of Sub-wavelength Grating

It has been well documented in the literature that the interferometry phenomena, which is associated with the Achromatic Grating Interferometer, functions using two grating structures to create an interference pattern [5]. In sub-wavelength gratings (SWG), the smallest grating period is less than the reconstruction wavelength ( $\Lambda/\lambda < 1$ ) and can operate in either the reflection or transmission regime, having only the zero forward or backward orders “*all other higher diffraction orders being evanescent*” [6].

In ref. [7], however, the  $m^{\text{th}}$  order diffraction angle  $\theta_m$  of a grating with period  $\Lambda$  and incidence angle  $\theta_i$  is given by:

$$\sin \theta_m = \sin \theta_i - m\lambda/\Lambda. \quad (1)$$

Further, because  $\Lambda$  is much less than  $\lambda$  for a SWG period, only the 0<sup>th</sup> ( $\theta_0$ ) and 1<sup>st</sup> order ( $\theta_1$ ) diffraction can occur, when  $\theta_i \geq 0$ . If the Bragg condition, which describes constructive interference through crystal lattice light scattering, is met,  $\theta_i = -\theta_1$ , that is equal but opposite in sign and,

$$\theta_i = \sin^{-1} \lambda/2\Lambda. \quad (2)$$

### B. Principle of Bidiffractive Grating

The bidiffractive grating (BDG) is a composite grating design that performs the functions of both input and output coupling of light into and out of an optical waveguide, through the superposition of two SWG doubly exposed holographic sinusoid relief gratings (see Fig. 1) [8-11].

The frequency spectrum of the BDG coupler contains two fundamental space-harmonics with the bidiffractive structure located on top of the sensor substrate where through the superposition of two parallel gratings  $G_a$  and  $G_b$ , the space-harmonics are made bi-directional where the bidiffractive structure continuously decouples the two fundamental space-harmonic frequencies into different directions at angles,  $\alpha$  for  $G_a$  and,  $\beta$  for  $G_b$ , for both transmission and reflection.

A continuous decoupling along the waveguide that is characterised by a certain leakage distance also occurs. The differential coupling scheme is realized through  $G_b$  coupling of the TE mode incident from left, and  $G_a$  coupling of the TM mode from right. For decoupling, the assignment for the TE

and TM modes to  $G_a$  and  $G_b$  is the reverse of the input coupling scheme (see Fig. 2).

The angles of incidence for both beams to meet the required resonance conditions for coupling is given by,

$$\sin \alpha = N_{TE} - \lambda/\Lambda_b \text{ and, } \sin \beta = N_{TM} - \lambda/\Lambda_a. \quad (3)$$

For the decoupling angles  $\varphi_{TE}$  and  $\varphi_{TM}$ , the following conditions apply,

$$\sin \varphi_{TE} = N_{TE} - \lambda/\Lambda_a \text{ and, } \sin \varphi_{TM} = N_{TM} - \lambda/\Lambda_b. \quad (4)$$

The coupling conditions for input coupling via  $G_a$  and output coupling via  $G_b$  and assuming 1<sup>st</sup> order coupling is given by,

$$\sin \alpha \pm \lambda/\Lambda_a = \pm N = -\sin \beta \pm \lambda/\Lambda_b. \quad (5)$$

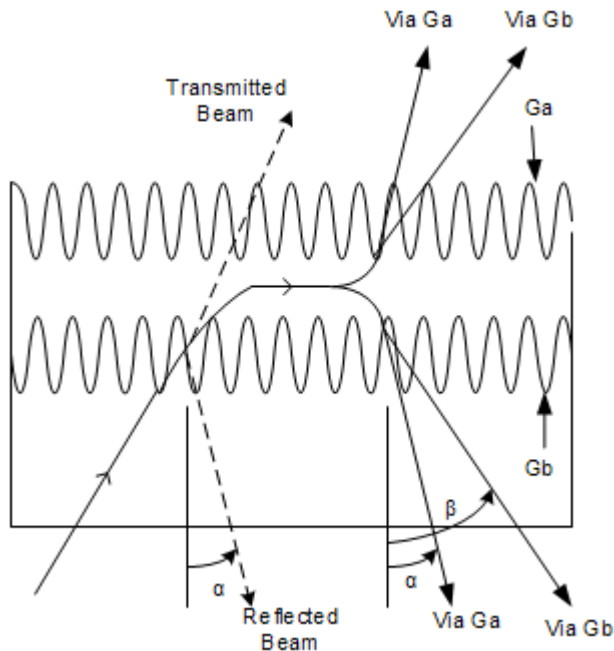


Fig. 1 The bidiffractive grating mechanism [8].

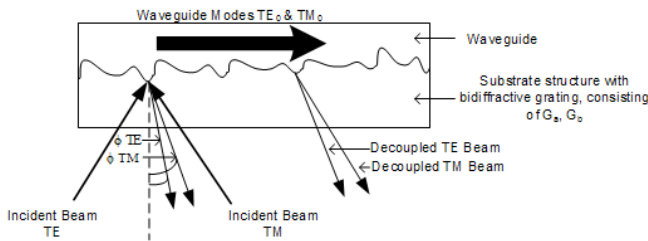


Fig. 2 Angle configuration for sensor device [9].

### C. Experimental Background of BDG Sensor

The experimental setup reported in ref. [10, 12] consists of the BDG (evanescent wave) label free sensor design where a change in refractive index of the penetration depth of the surface wave causes a phase velocity change of the individual

modes with the outcoupling of the relative phase monitored through imaging the output onto a CCD detector (see Fig. 3).

The outcoupled modes are imaged onto a CCD detector by means of a lens and sheet polarizer that generates an interference pattern proportional to the relative phase velocity of the two surface waves that can be evaluated using the method of Fourier transform spectroscopy.

Because of the materials chosen, the disposable sensor chip incorporates an integrated microcell contacted to the (Polymer) substrate edges that contains a 1 mm × 5 mm sample fluid flow channel of thickness 40 μm containing a volume of 0.2 μl above the sensor surface, transported by low pressure nitrogen at a flow rate of 30 μl min<sup>-1</sup>.

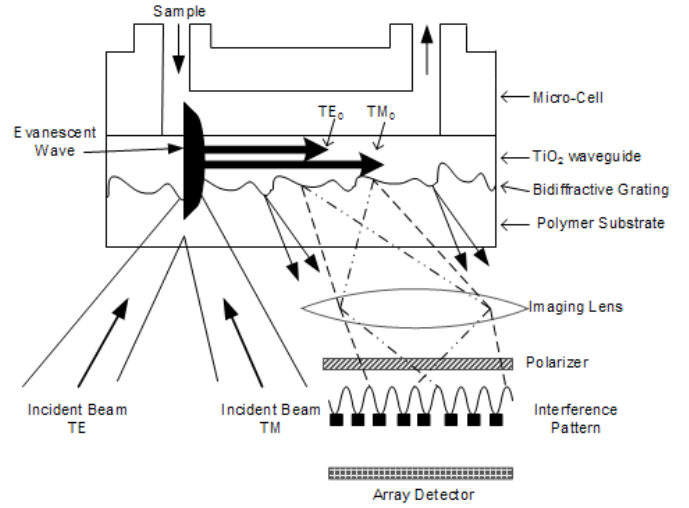


Fig. 3 Principle of operation of BDG sensor [10].

### D. Principle of Holographic Grating Manufacture

A simple approach to double exposure holography is to illuminate a surface with two differently inclined plane waves each with the same amplitude and wavelength so that the amplitude distribution results in the xy plane described by,

$$A \exp(ik_1x) + A \exp(ik_2x), \quad (6)$$

where  $k_1 = (2\pi/\lambda)\sin\theta_1$ ,  $k_2 = (2\pi/\lambda)\sin\theta_2$ , and  $\theta_1$  and  $\theta_2$  are the incident angles. [13]

The Lloyd's Mirror arrangement (see Fig. 4) is used by many researchers and experimenters in photolithographic techniques to produce optical diffraction gratings [14]. One arm of the mirror arrangement is a light sensitive photographic emulsion (or photoresist) applied to a substrate that is intended to support a diffraction grating following a photo etching or development process.

Light strikes the photoresist from two independent paths, one directly from the source and the other via the longer path provided from the source to a mirror together with the distance represented by the reflection from the mirror to the photoresist. As a result the incidence and reflected beams meet at the surface with constructive and destructive interference to create a sinusoidal intensity pattern in the photoresist the period of which is determined by the angle theta. This angle theta is variable as the Lloyd's mirror configuration is

mounted on a rotational base to alter the angle at which the incident and reflected beams strikes the surfaces.

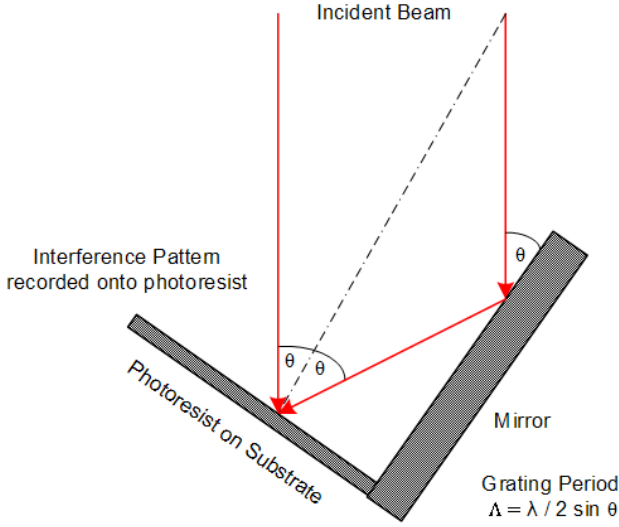


Fig. 4 Principle of Lloyd mirror holography [14].

#### E. A Simplified Two Dimensional BDG Geometric Model

For a holographic exposure laser wavelength of  $\lambda = 442$  nm, we can determine the angle  $\angle \alpha$  for a given grating period for example, if we let  $\alpha_1 = 45^\circ$  and  $\alpha_2 = 37.5^\circ$  then,

$$a_1 = 442 \text{ nm} / 2 \sin 45 = 312 \text{ nm} \quad (7)$$

$$a_2 = 442 \text{ nm} / 2 \sin 37.5 = 363 \text{ nm} \quad (8)$$

These calculated values correlate well with the experimental grating periods reported in ref. [11] namely, 314 nm and 362 nm.

For the purposes of modeling, the conceptualization of a BDG may be considered along the lines of the description in [15] that uses a rectangular profile to achieve an outcome similar to that of [8]. The principle of the bidirectional coupler of [15] is based on a grating structure divided into cells where each cell contains a number of grating lines of constant period,  $\Lambda$ , that is equal for all cells (see Fig. 5).

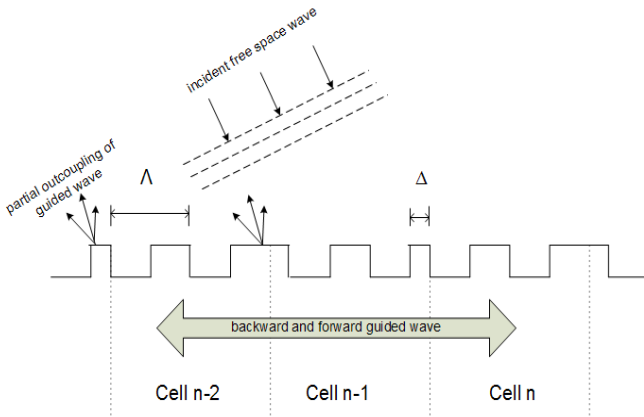


Fig. 5 Bi-directional coupling grating model [15].

However, when each cell is dislocated from its neighbouring cells by a distance factor,  $\Delta$ , this imposes a phase modulation of the in-coupled light that makes partial outcoupling of the guided wave possible. Assuming we use the grating parameters of [11] namely 314 nm and 362, then  $\Delta = 48$  nm. Further assuming that for modelling and simulation purposes the light source will be a HeNe Laser with  $\lambda = 632.8$  nm, we assume our grating period for modelling to be  $\lambda / 2 \sim 315$  nm and set  $\Delta = 50$  nm, to simplify the geometry involved.

In principle therefore, a simplified and more practical model has been developed for computer modelling and simulation of a self contained input output coupling mechanism to provide the light excitation required for SPR and recovering any phase shifts resulting from changes in refractive index at the sensor surface.

### III. MULTIPHYSICS MODELING

The bi-directional grating coupled SPR sensor using In-Plane Hybrid-Mode Waves was modelled and simulated to determine the EM field distribution of the multilayer stack. The modelling and simulation were carried out in COMSOL using the RF module as described in the following.

#### A. Geometry, Boundary Conditions, and Material Properties

A 10 element binary-phase (blazed) grating geometry was modelled (see Fig. 6) in order to allow sufficient grating length to establish input output coupling and generation of an evanescent wave for surface plasmon excitation in the top gold layer of the multilayer stack.

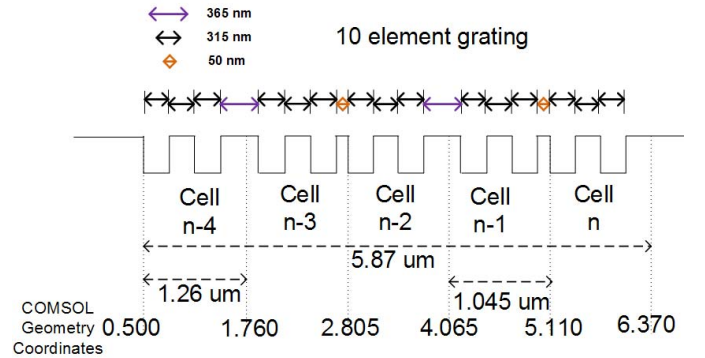


Fig. 6 The 10 element grating geometry used.

Illumination from the bottom boundary of the stack was described as a Port boundary condition specifying the  $\mathbf{H}$  field as a HeNe Laser source ( $\lambda_0 = 0.6328 \mu\text{m}$ ) with in-plane polarization ( $w_0 = 0.005 \mu\text{m}$  FWHM Beamwidth), wavenumber ( $k_0 = 2\pi/\lambda_0$ ) at a specified angle of incidence.

The periodic nature of the nature of the problem was described through the combination of *Floquet* boundary conditions in concert with the Port boundary condition, the Floquet boundary condition being critical to Finite Element Method (FEM) modelling as it indicates the main distinction between leaky waves along periodic structures and multilayer structures, through a single propagation factor,  $k_p$ . [16].

Table I describes the applied material refractive indices (RI) for the multilayer structure.

TABLE I  
OPTICAL PROPERTIES - MULTILAYER MATERIALS

Material	Layer	RI ( $n$ )	Source
Polycarbonate	Substrate $n_{\text{sub}}$	1.586	[17]
Titanium Dioxide ( $\text{TiO}_2$ )	Waveguide $n_{\text{film}}$	2.584	[18]
Gold (Au) @ 632.8 nm	Gold $n_{\text{gold}}$	0.19715	[19]
Air	Air $n_{\text{cover}}$	1.0	NA

Some additional COMSOL and FEM modeling techniques were required namely,

1. The concept and application of ‘Assembly versus Composite Geometry’,
2. Application of ‘Identity Pairs’ at the boundaries of assemblies to establish source and destination boundaries for an excitation source,
3. Application of the ‘Floquet Boundary Conditions’ as previously outlined.
4. Setting the port conditions for the identity pairs outlined in 2.

The model geometry (see Fig. 7) was extended to include additional layers (Air  $n = 1$ ) below the Polycarbonate substrate to serve as the source and destination for the excitation  $p$ -polarized laser source.

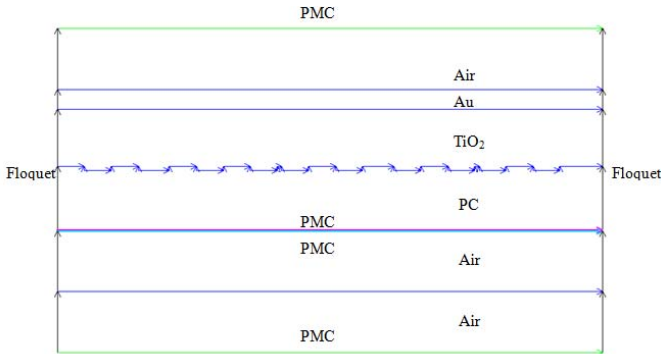


Fig. 7 Final model geometry and boundary conditions.

The left and right external boundaries were set up with Floquet conditions and the upper and lower external boundaries together with the identity pair boundary were set as perfect magnetic conductors (PMC). The internal boundaries all remained as *continuity*.

### B. Simulation Results

The resulting plots (see Figs. 8 and 9) show source and return waves from and into the air region below the substrate, together with the scattering effect at the diffraction grating, and the required surface plasmon excitation above the gold region penetrating approximately 100+ nm into the air region.

The surface plot for time averaged power (Fig. 10) shows the greatest power distribution occurring within the gold layer and also provides evidence for the reasonable assumptions of Goos-Hänchen shift together with forward and backward propagation within the waveguide layer.

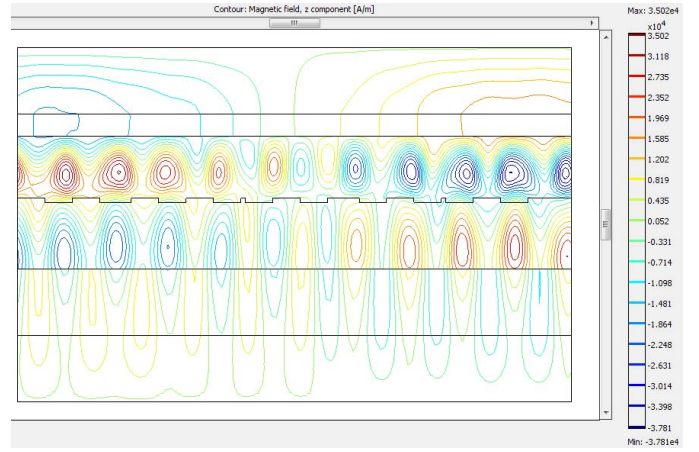


Fig. 8 Contour plot, magnetic field, z component (A/m).

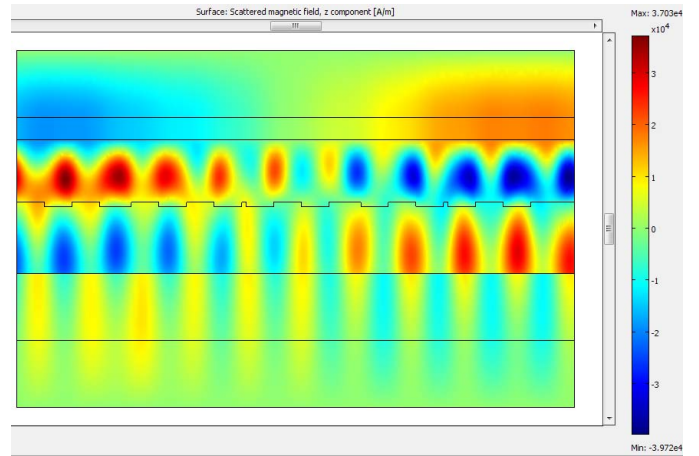


Fig. 9 Surface plot, scattered magnetic field, z component (A/m).

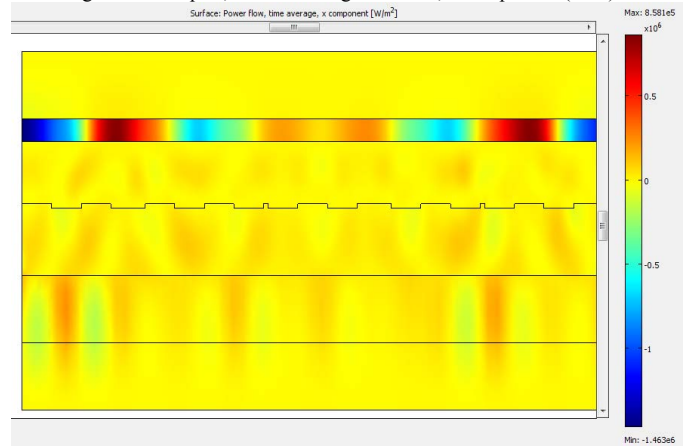


Fig. 10 Surface plot, Power, time average ( $\text{W}/\text{m}^2$ )

## IV. DISCUSSION

In this paper we have described a novel design of a grating coupled optical waveguide SP excitation mechanism loosely based on a prior design described in ref. [8] that differs in that unlike the prior design, it may not be limited to a dual exposure holographic construction method of superimposition of sinusoids to establish the grating profile.

The results of the finite element modelling presented suggests that superimposed SWG grating profiles other than sinusoidal ones also exhibit input-output coupling of light which opens up the possibility of considering alternative construction methods for better reproducibility and enhanced energy transfer performance and signal to noise ratio.

## V. CONCLUSIONS

The results of the FEM modeling and simulation performed confirmed the credibility of the design concepts such that further research and development is warranted, particularly with respect to extending the FEM modelling to analyse the signal decoupling characteristics and the effect of refractive index variations in the top (analyte) layer.

Never-the-less, we view a future physical representation of this device configuration as potentially offering significant improvements in the practicality of future generations of SPR field deployable bio-sensing instruments for a variety of applications including remote point-of-delivery medical diagnostics.

## APPENDIX

### A. Multilayer Stack Dimensions

Table II presents the dimensions used to create the multilayer stack and grating geometry in COMSOL. Extra x represents the x-axis spacing's for the grating, whilst Extra y indicates the thickness of each of the layers, with  $y = 0.15$  and  $y = 0.16$  representing the grating height of 10 nm.

TABLE II  
2D MULTILAYER STACK AND GRATING GEOMETRY DIMENSIONS

Axis ( $\mu\text{m}$ )		Grid	
x min	0.25	x spacing	0.25
x max	7.5	Extra x	0.815, 1.13, 1.445, 1.81, 2.125, 2.44, 2.755, 2.805, 3.07, 3.12, 3.435, 3.75, 4.065, 4.43, 4.745, 5.06, 5.375, 5.425, 5.74, 6.055, 6.37, 6.87
y min	-0.02	y spacing	0.02
y max	0.4	Extra y	-0.3, -0.15, 0.15, 0.16, 0.30, 0.35, 0.5

From Table II, layer thicknesses from bottom to top are:

- Air 150 nm
- Air 150 nm
- PC 150 - 160 nm (includes grating profile)
- $\text{TiO}_2$  140 – 150 nm (includes grating profile)
- Au 50 nm
- Air 150 nm

### B. Boundary Condition Formulae and Port Settings

1. Floquet:  $\mathbf{E}_{DST} = \mathbf{E}_{SRC} \exp(-j\mathbf{k} \cdot (\mathbf{r}_{DST} - \mathbf{r}_{SRC}))$
2. PMC:  $\mathbf{n} \times \mathbf{H} = 0$
3. Continuity:  $(\mathbf{n} \times (\mathbf{H}_1 - \mathbf{H}_2))_z = 0; (\mathbf{n} \times (\mathbf{E}_1 - \mathbf{E}_2))_z = 0$

The two PMC internal boundaries (Air-PC) are configured as an "Identity Pair" to establish the Port required for the wave excitation source with port power level  $P_{in} = 1\text{W}$ , port phase  $\square_p = 0$ . The port mode specification is set to Analytic, Transverse Magnetic (TM), Mode Number =1.

## ACKNOWLEDGMENT

The authors greatly appreciate the assistance of PhD candidate Daryoush Mortazavi of the BioMEMS Research Group, Deakin University in literature review activities and, John Cameron, Senior Lecturer, School of Information Technology, Deakin University for assistance with the mathematical constructs for blazed gratings.

## REFERENCES

- [1] E. Kretschmann and H. Raether, "Radiative decay of non-radiative surface plasmons excited by light," *Zeitschrift für Naturforschung*, vol. 23, pp. 2135-2136, 1968.
- [2] M. S. Islam, A. Z. Kouzani, X. J. Dai, and W. P. Michalski, "Parameter sensitivity analysis of surface plasmon resonance biosensor through numerical simulation," in *Proceedings of 2010 IEEE/ICME International Conference on Complex Medical Engineering (CME2010)*, Gold Coast, Australia, 2010.
- [3] B. A. Sexton, B. N. Feltis, and T. J. Davis, "Characterisation of gold surface plasmon resonance sensor substrates," *Sensors and Actuators A: Physical*, vol. 141, pp. 471-475, 2008.
- [4] B. N. Feltis, B. A. Sexton, F. L. Glenn, M. J. Best, M. Wilkins, and T. J. Davis, "A hand-held surface plasmon resonance biosensor for the detection of ricin and other biological agents," *Biosensors and Bioelectronics*, vol. 23, pp. 1131-1136, 2008.
- [5] K. Buchwald, "Fused Silica Transmission Gratings," Ibsen Photonics, 2007.
- [6] B. Kress and P. Meyrueis, *Applied digital optics : micro-optics, optical MEMS, and nanophotonics*. Chichester, West Sussex, U.K. ; Hoboken, N.J.: Wiley, 2009.
- [7] M. Shiozaki and M. Shigehara, "Novel Design of Polarization Independent Multi-layer Diffraction Grating with High Angular Dispersion," *SEI Technical Review*, vol. 59, 2005.
- [8] C. Fattinger, "The bidiffractive grating coupler," *Applied Physics Letters*, vol. 62, p. 1460, 1993.
- [9] C. Fattinger, B. Danielzik, W. Ehrfeld, M. Heming, H. Lowe, A. Michel, F. Michel, N. Oranth, and J. Spinke, "A Universal Transducer for Optical Interface Analytics: Transducer Design and Concepts for Economical Mass Production," in *Thin Films on Glass*, Bach - Neuroth, Ed.: Springer-Verlag, 1997.
- [10] J. Spinke, N. Oranth, C. Fattinger, H. Koller, C. Mangold, and D. Voegelin, "The bidiffractive grating coupler: application to immunosensing," *Sensors and Actuators B: Chemical*, vol. 39, pp. 256-260, 1997/4// 1997.
- [11] C. Fattinger, H. Schuetz, M. Gale, and C. Mangold, "Bidiffractive grating coupler: universal transducer for optical interface analytics " *Optical Engineering*, vol. 34, pp. 2744-2753, 1995.
- [12] T. O'Brien, L. H. Johnson Iii, J. L. Aldrich, S. G. Allen, L.-T. Liang, A. L. Plummer, S. J. Krak, and A. A. Boiarski, "The development of immunoassays to four biological threat agents in a bidiffractive grating biosensor," *Biosensors and Bioelectronics*, vol. 14, pp. 815-828, 2000.
- [13] F. Gori and G. Guattari, "Time-ordered doubled-exposure holography," *Optics Communications*, vol. 5, pp. 359-361, 1972.
- [14] M. C. Marconi and P. W. Wachulak, "Extreme ultraviolet lithography with table top lasers," *Progress in Quantum Electronics*, vol. 34, pp. 173-190.
- [15] J. Backlund, J. Bengtsson, C. F. Carlstrom, and A. Larsson, "Multifunctional grating couplers for bidirectional incoupling into planar waveguides," *Photonics Technology Letters, IEEE*, vol. 12, pp. 314-316, 2000.
- [16] T. Tamir and H. L. Bertoni, "Lateral Displacement of Optical Beams at Multilayered and Periodic Structures," *J. Opt. Soc. Am.*, vol. 61, pp. 1397-1413, 1971.
- [17] J. E. Mark, *Polymer Data Handbook*. International: Oxford University Press, 1999.
- [18] M. J. Weber, *Handbook of optical materials*. Boca Raton, FL: CRC Press, 2003.
- [19] E. D. Palik, *Handbook of Optical Constants* vol. 1: Academic Press, 1998.